Measurement of forward $Z \rightarrow e^+e^-$ production at $\sqrt{s} = 8\,\text{TeV}$

The LHCb collaboration

E-mail: drw1@cam.ac.uk

ABSTRACT: A measurement of the cross-section for Z-boson production in the forward region of pp collisions at 8 TeV centre-of-mass energy is presented. The measurement is based on a sample of $Z \rightarrow e^+e^-$ decays reconstructed using the LHCb detector, corresponding to an integrated luminosity of $2.0\,\text{fb}^{-1}$. The acceptance is defined by the requirements $2.0 < \eta < 4.5$ and $p_\text{T} > 20\,\text{GeV}$ for the pseudorapidities and transverse momenta of the leptons. Their invariant mass is required to lie in the range 60–120 GeV. The cross-section is determined to be

$$\sigma(\text{pp} \rightarrow Z \rightarrow e^+e^-) = 93.81 \pm 0.41(\text{stat}) \pm 1.48(\text{syst}) \pm 1.14(\text{lumi})\,\text{pb}\,,$$

where the first uncertainty is statistical and the second reflects all systematic effects apart from that arising from the luminosity, which is given as the third uncertainty. Differential cross-sections are presented as functions of the Z-boson rapidity and of the angular variable ϕ^*, which is related to the Z-boson transverse momentum.

KEYWORDS: Electroweak interaction, QCD, Forward physics, Hadron-Hadron Scattering, proton-proton scattering

Contents

1 Introduction

Measurements of vector boson production in hadron collisions permit tests of electroweak physics and of QCD. The effective kinematic range of the LHCb detector [1], approximately $2.0 < \eta < 4.5$ where η is the pseudorapidity, complements that of the general purpose LHC detectors whose acceptance for precise measurements extends to $|\eta| \approx 2.5$. Measurements at LHCb are sensitive to the knowledge of the proton structure functions at very low Bjorken x values, where the parton distribution functions (PDFs) are not well constrained by previous data, or by other LHC experiments [2].

The most straightforward decay mode in which LHCb can study the production of the Z boson is the channel $Z \to \mu^+\mu^-$ [3], since the experiment has a highly efficient trigger and precise reconstruction capabilities for high-momentum muons. However, it is also desirable to examine the channel $Z \to e^+e^-$,[1] which offers a statistically independent sample, with substantially different sources of systematic uncertainties. The main difficulty with electron reconstruction in LHCb is the energy measurement. A significant amount of material is traversed by the particles before they reach the magnet, and their measured momenta are therefore frequently reduced by bremsstrahlung, which cannot be recovered fully using the calorimeters because of saturation at an energy corresponding to a transverse momentum of around 10 GeV per channel. Consequently the initial electron directions are well determined, but their measured momenta are low by a variable amount, $\sim 25\%$ on average. Therefore the rapidity of the Z boson, y_Z, is well determined while its transverse momentum, p_T, is

---

[1]Throughout this note we use $Z \to e^+e^-$ to imply the formation of e^+e^- through either a Z or a virtual photon γ^*, including the effect of their interference.

poorly measured and biased. Thus, as in ref. [4], the distribution of the angular variable ϕ^*, which is correlated with p_T but less affected by bremsstrahlung, is studied. The ϕ^* variable [5] is defined in terms of the directions of the particle momenta

$$\phi^* \equiv \frac{\tan(\phi_{\mathrm{acop}}/2)}{\cosh(\Delta\eta/2)} \approx \frac{p_T}{M} \, ,$$

where $\Delta\eta$ is the difference in pseudorapidity between the leptons, the acoplanarity angle $\phi_{\mathrm{acop}} = \pi - |\Delta\phi|$ depends on the difference between the azimuthal directions of the lepton momenta, $\Delta\phi$, and M and p_T are the invariant mass and transverse momentum of the lepton pair.[2]

In this paper, we present a measurement of the cross-section for pp $\to$ Z $\to$ e$^+$e$^-$ using the data recorded by LHCb in 2012 at $\sqrt{s} = 8\,\mathrm{TeV}$, corresponding to an integrated luminosity of $2.0\,\mathrm{fb}^{-1}$. The approach is essentially the same as that used in a previous study of the same channel at $\sqrt{s} = 7\,\mathrm{TeV}$ [4]. The current measurement, as well as being at a higher centre-of-mass energy, benefits from a significantly higher and more precisely determined integrated luminosity, and from stable trigger conditions. Futhermore, an improved Monte Carlo simulation of the detector and an improved modelling of electron bremsstrahlung are available. The determination is performed in the same kinematic region as the LHCb measurement of Z $\to$ $\mu^+\mu^-$ [3], namely $60 < M(\mathrm{Z}) < 120\,\mathrm{GeV}$ and $2.0 < \eta < 4.5$ and $p_T > 20\,\mathrm{GeV}$ for the leptons.

Section 2 gives a brief description of the detector, triggers and software, after which section 3 describes the event selection and the analysis procedure, and section 4 explains the techniques used for determining the main uncertainties in the measurement. The results are presented in section 5 followed by a brief summary in section 6.

2   Detector and simulation

The LHCb detector [1, 6] is a single-arm forward spectrometer designed for the study of particles containing b or c quarks. The detector includes a high-precision tracking system consisting of a silicon-strip vertex detector surrounding the pp interaction region, a large-area silicon-strip detector located upstream of a dipole magnet with a bending power of about $4\,\mathrm{Tm}$, and three stations of silicon-strip detectors and straw drift tubes, placed downstream of the magnet. The tracking system provides a measurement of momentum, p, with a relative uncertainty that varies from 0.5% at low momentum to 1.0% at $200\,\mathrm{GeV}$. The minimum distance of a track to a primary vertex, the impact parameter, is measured with a resolution of $(15 + 29/p_T)\,\mu\mathrm{m}$, where p_T is in GeV. Different types of charged hadrons are distinguished using information from two ring-imaging Cherenkov detectors. Photon, electron and hadron candidates are identified by a calorimeter system consisting of scintillating-pad (SPD) and preshower (PRS) detectors, an electromagnetic calorimeter (ECAL) and a hadronic calorimeter (HCAL). Muons are identified by a system composed of alternating layers of iron and multiwire proportional chambers.

---

[2]Natural units with $\hbar = c = 1$ are used throughout, so that mass and momentum are measured in units of energy.

The trigger consists of a hardware stage, based on information from the calorimeter and muon systems, followed by a software stage, which applies a full event reconstruction. Events are first required to pass the hardware trigger for electrons, which selects events having an electromagnetic cluster of high transverse energy geometrically associated with signals in the PRS and SPD detectors. This high-p_{T} single-electron trigger is then refined by the software trigger. Global event cuts on the numbers of hits in several detectors, such as the SPD, are applied in order to prevent high-multiplicity events from dominating the processing time.

Simulated event samples of $\mathrm{Z} \to \mathrm{e^+e^-}$ with $M(\mathrm{e^+e^-}) > 40\,\mathrm{GeV}$ are used in the analysis. Simulated samples of $\mathrm{Z} \to \tau^+\tau^-$, $\mathrm{t\bar{t}}$, $\mathrm{W^+W^-}$ and $\mathrm{W^{\pm}Z}$ are used to assess possible background contributions. In the simulation, pp collisions are generated using PYTHIA 8.1 [7, 8] with a specific LHCb configuration [9]. The interaction of the generated particles with the detector and its response are implemented using the GEANT4 toolkit [10, 11] as described in ref. [12].

3 Data analysis

The reconstructed particles used as the basis of the analysis satisfy basic track quality requirements. The following criteria are applied in order to refine the sample of candidates for analysis:

- either the electron or the positron candidate should satisfy a single-electron trigger at all stages of the trigger;

- the reconstructed electron and positron candidates should have pseudorapidity and transverse momentum satisfying $2.0 < \eta < 4.5$ and $p_{\mathrm{T}} > 20\,\mathrm{GeV}$ respectively. The reconstructed $\mathrm{e^+e^-}$ invariant mass should be greater than $40\,\mathrm{GeV}$;

- to ensure good track quality, the electron and positron candidates should have momenta measured with estimated fractional uncertainty smaller than 10%;

- in order to identify the particles as electron candidates, both are required to show associated energy deposition in the calorimeters characteristic of high-energy electrons, namely $E_{\mathrm{ECAL}}/p > 0.1$, $E_{\mathrm{HCAL}}/p < 0.05$ and $E_{\mathrm{PRS}} > 50\,\mathrm{MeV}$ where E_{ECAL}, E_{HCAL} and E_{PRS} denote the energies recorded in the electromagnetic calorimeter, hadronic calorimeter and preshower detector respectively;

- if more than one $\mathrm{e^+e^-}$ pair satisfies the above criteria in an event (which occurs in approximately 0.7% of cases), one is selected at random.

Applying these selection requirements on data, $65\,552$ $\mathrm{Z} \to \mathrm{e^+e^-}$ candidates are obtained. Most backgrounds are removed by subtracting a sample of same-sign $\mathrm{e^{\pm}e^{\pm}}$ candidates. The validity of this procedure is assessed in section 4. Applying identical selection criteria, 4595 same-sign candidates are found.

The cross-section is determined using the following expression:

$$\sigma = \frac{N(\mathrm{e^+e^-}) - N(\mathrm{e^{\pm}e^{\pm}}) - N_{\mathrm{bg}}}{\epsilon \cdot \int \mathcal{L}\mathrm{d}t} \cdot f_{\mathrm{MZ}}, \tag{3.1}$$

where $N(\mathrm{e^+e^-})$ is the number of signal candidates selected in data, $N(\mathrm{e^\pm e^\pm})$ is the number of same-sign candidates, N_{bg} is the expected background not covered by same-sign candidates (predominantly $\mathrm{Z} \to \tau^+\tau^-$) taken from simulation and $\int \mathcal{L}dt$ is the integrated luminosity. The event detection efficiency, ϵ, is evaluated using a combination of data and simulation as explained below, and refers to events for which the true electrons satisfy $2.0 < \eta < 4.5$, $p_{\mathrm{T}} > 20\,\mathrm{GeV}$ and $60 < M(\mathrm{e^+e^-}) < 120\,\mathrm{GeV}$. The factor f_{MZ} (determined from simulation) corrects for the inclusion in the data sample of $\mathrm{Z} \to \mathrm{e^+e^-}$ candidates that pass the event selection even though their true mass lies outside the range $60 < M(\mathrm{e^+e^-}) < 120\,\mathrm{GeV}$. The correction procedure is applied for 17 bins in Z rapidity in the range $2.00 < y_{\mathrm{Z}} < 4.25$.[3] The analysis is also performed for 15 bins in ϕ^*. The choice of binning takes account of the available sample size and the resolutions achieved on y_{Z} and ϕ^*. The luminosity is obtained with an overall uncertainty of 1.2% [13].

The efficiency of the event selection is factorised into several components,

$$\epsilon = \epsilon_{\mathrm{track}} \cdot \epsilon_{\mathrm{kin}} \cdot \epsilon_{\mathrm{PID}} \cdot \epsilon_{\mathrm{GEC}} \cdot \epsilon_{\mathrm{trig}} . \tag{3.2}$$

The efficiencies are determined such that the efficiency for each stage of the analysis is estimated for events that pass the preceding stages. Thus, $\epsilon_{\mathrm{track}}$ is the efficiency associated with the reconstruction of both electrons as tracks satisfying the quality requirements and ϵ_{kin} gives the efficiency that both these reconstructed electron tracks satisfy the kinematic acceptance requirements on p_{T} and η. Similarly, ϵ_{PID} is the efficiency for identification of the tracks as electrons, ϵ_{GEC} is the estimated efficiency of the global event cuts for these events and ϵ_{trig} is the trigger efficiency. The determination of these contributions to the efficiency is performed separately in each bin of y_{Z} or of ϕ^*. The contributions that the terms in the efficiency make to the systematic uncertainty on the measurement are summarised in section 4.

The tracking efficiency, $\epsilon_{\mathrm{track}}$, gives the probability that, in events in which the electrons satisfy $2.0 < \eta < 4.5$, $p_{\mathrm{T}} > 20\,\mathrm{GeV}$ and $60 < M(\mathrm{e^+e^-}) < 120\,\mathrm{GeV}$ at the particle level (*i.e.* based on their true momenta, as known in simulated events), both of them correspond to reconstructed tracks satisfying the track quality requirements. In order to characterise accurately the dependence of the efficiency on y_{Z} and ϕ^*, the efficiency is taken from simulation. A consistency check using data allows a systematic uncertainty to be assigned as described in section 4. The efficiency shows a significant dependence on y_{Z}, but almost no variation with ϕ^*.

The kinematic efficiency, ϵ_{kin}, accounts for the possibility that a $\mathrm{Z} \to \mathrm{e^+e^-}$ decay in which the electron momenta at particle level satisfy the kinematic requirements on p_{T} and η may not do so for the reconstructed momenta, even though the tracks are reconstructed and satisfy the track quality requirements. This is a sizeable correction because of bremsstrahlung. The efficiency is determined using simulated events, with data used to assess the systematic uncertainty as described in section 4. In contrast to the earlier analysis [4], the particle-level electron momentum used here is the momentum before

---

[3]Although tracks can be reconstructed at larger rapidities, the efficiency for electron identification vanishes just above $y_{\mathrm{Z}} = 4.25$ because of the inner edge of the calorimeter acceptance, so that no candidate event at higher rapidity survives in either data or simulation.

final-state radiation (FSR), so that the kinematic efficiency also includes the effect of FSR as implemented in PYTHIA 8.1, and an additional correction is no longer applied.

The particle identification efficiency, ϵ_{PID}, accounts for the possibility that a signal event passing all track finding and kinematic requirements fails the electron identification requirements, either because the track falls outside the calorimeter acceptance, or because the requirements on calorimeter energies are not satisfied. The overall efficiency is taken from simulation in order to model accurately a significant dependence on y_Z. This dependence is a consequence of the geometrical acceptance and is assumed to be modelled reliably. The efficiency of the calorimeter energy requirements is validated using data as described in section 4, leading to a systematic uncertainty.

The only global event cut that has any significant effect on the $Z \to e^+e^-$ channel is a requirement in the electron triggers that the number of hits in the SPD be less than 600. In order to assess the consequent loss of events, use is made of $Z \to \mu^+\mu^-$ events that satisfy the dimuon trigger, for which the number of SPD hits, N_{SPD}, is required to be less than 900. The distribution of N_{SPD} in dielectron events should be the same as that in dimuon events apart from the contribution from the leptons. In the region $N_{\mathrm{SPD}} < 600$ it is observed that the distribution for $Z \to e^+e^-$ is consistent with that for $Z \to \mu^+\mu^-$ with an upward shift of 10 ± 5 hits associated with showering of the electron and positron. This shift is confirmed in simulation. Accordingly, we use the fraction of $Z \to \mu^+\mu^-$ dimuon triggers in the range $590 \leq N_{\mathrm{SPD}} < 900$ to estimate the loss of dielectron events in the range $600 \leq N_{\mathrm{SPD}} < 910$. The small fraction of dimuon events having $N_{\mathrm{SPD}} \geq 900$ is estimated to be 0.7% by extrapolation using an empirical fit to the distribution. The efficiency shows a weak dependence on Z rapidity and ϕ^*.

The trigger efficiencies for events passing the selection cuts are determined from data using a "tag-and-probe" method. The principle is to use events in which the electron satisfies the trigger to determine the efficiency for the positron to satisfy the trigger and vice versa.

The values of the various correction factors, averaged over all values of y_Z, are summarised in table 1. The uncorrelated components of the uncertainties are generally related to the statistical uncertainty associated with each efficiency. These can be sizeable in individual bins, but become small when their effect on the integrated cross-section is considered. The correlated components are taken to be fully correlated between bins, and therefore have roughly the same effect on individual bins and on the integrated cross-section. The principal systematic uncertainties are discussed in greater detail in section 4. The overall efficiency is shown as a function of y_Z and ϕ^* in figure 1.

4 Systematic uncertainties

The tracking efficiency is evaluated using simulation and checked using data. The principle is to search for events where a track appears to be missing, so that the signature of a Z becomes a high-p_T electron track accompanied by a high-energy ECAL cluster with no associated track. An efficiency is determined by comparison with the corresponding number of events in which two tracks are reconstructed. To reduce background, more
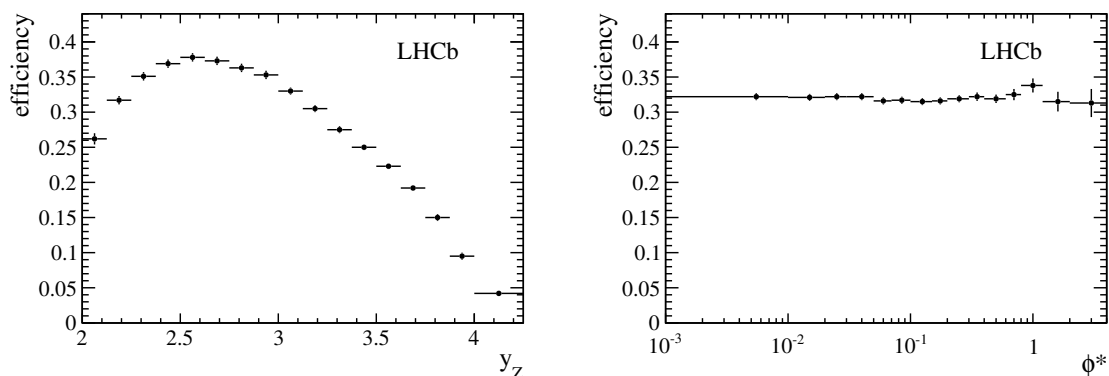
Figure 1. Overall detection efficiency, ϵ, determined from a combination of data and simulation as described in the text, shown as a function of (left) y_Z and (right) ϕ^*.

	Average value	Fractional uncertainty Uncorrelated	Correlated
ϵ_{track}	0.912	0.001	0.010
ϵ_{kin}	0.507	0.002	0.006
ϵ_{PID}	0.838	0.001	0.007
ϵ_{GEC}	0.916	—	0.006
ϵ_{trig}	0.892	0.001	—
ϵ	0.319	0.002	0.016
f_{MZ}	0.969	0.001	—
Background estimation	—	—	0.004
$\int \mathcal{L}\mathrm{d}t \, / \, \mathrm{pb}^{-1}$	1976	—	0.012

Table 1. Efficiencies and other factors used for the cross-section determination (see eq. (3.1)) averaged over the experimental acceptance by integrating over y_Z. The fractional uncertainties on the overall factors are also given, separated into components that are assumed to be correlated and uncorrelated between bins of the differential distributions.

stringent particle identification requirements are imposed on the tag electron, and isolation requirements are imposed on both the electron and the ECAL cluster. This cannot be regarded as a direct measurement of the efficiency of the main analysis selection because more stringent requirements are employed. Instead, the same procedure is applied to the simulated event sample. The ratio between the two, 0.990 ± 0.004, is taken as a correction to ϵ_{track} obtained from simulation, with the full size of the correction taken as a systematic uncertainty, ± 0.010, which is assumed to be fully correlated between bins of the differential distributions.

The kinematic efficiency is also evaluated from simulation. Accurate simulation of the detector material is necessary in order to model correctly energy losses through bremsstrahlung, and any inaccuracy would lead to a scaling of the measured momenta. This is tested by examining the modelling of the p_{T} distributions by simulation, particularly in the neighbourhood of the 20 GeV threshold. Figure 2 shows the distribution of $\min(p_{\mathrm{T}}(\mathrm{e}^+), p_{\mathrm{T}}(\mathrm{e}^-))$
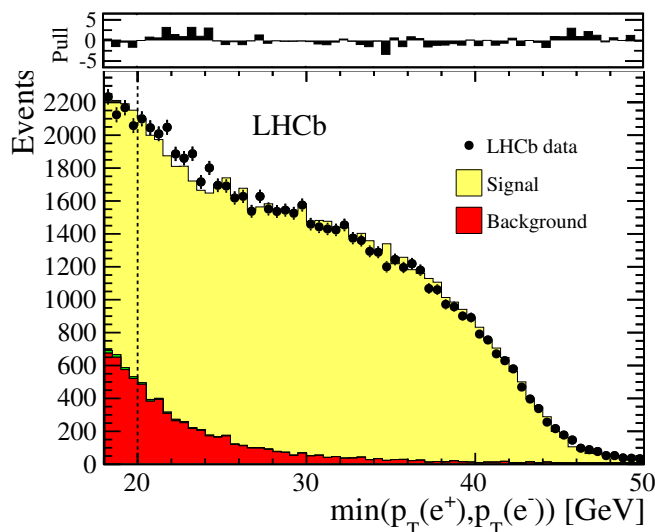
Figure 2. Comparison between data and simulation for the distribution of $\min(p_T(e^+), p_T(e^-))$, used in the assessment of uncertainties in ϵ_{kin}. The data are shown as points with error bars, the background obtained from same-sign data is shown in red (dark shading), to which the expectation from Z $\rightarrow e^+ e^-$ simulation is added in yellow (light shading). The simulated distribution is normalised to the background-subtracted data. The $\tau^+ \tau^-$ background is also included (green), though barely visible. The dashed line indicates the threshold applied in the event selection. The small plot at the top shows the pulls (*i.e.* deviations divided by statistical uncertainties) between the data and the expectation.

for data compared with simulation. In order to quantify the uncertainty in ϵ_{kin}, the p_T values in data are scaled by a global factor α to represent the effect of an uncertainty in the detector material. The χ^2 between data and simulation is examined as α is varied. The resulting uncertainty in α translates into a relative uncertainty in ϵ_{kin} of 0.6% (or 1.2% for $y_Z > 3.75$), which is taken to be a systematic uncertainty fully correlated between bins.

The contribution to ϵ_{PID} resulting from the calorimeter acceptance is purely geometrical and is assumed to be modelled reliably in simulation. To assess the reliability of simulation for the calorimeter energy requirements, events are selected in which one electron is tagged using the standard criteria, while a second probe track is found that satisfies all the requirements apart from that on the energy recorded in one of the calorimeters. By examining the distributions of calorimeter energy in the neighbourhood of the threshold applied, an estimate of any correction needed and its uncertainty is made. The test is repeated for each part of the calorimeter in turn. As a result of these studies, a systematic uncertainty of 0.7% on ϵ_{PID} is assigned, independent of y_Z and ϕ^*, and treated as fully correlated between bins.

The statistical uncertainty in the determination of ϵ_{GEC} is taken as part of the systematic uncertainties. The uncertainty in the 10 ± 5 N_{SPD} offset leads to an additional systematic uncertainty of 0.4% overall, while an uncertainty of 0.2% is assigned based on comparing various extrapolation techniques. The value of ϵ_{GEC} is determined as a function of y_Z and ϕ^*. The statistical uncertainty on the determination of ϵ_{trig} is treated as a systematic uncertainty.

The principal background to the selected $Z \rightarrow e^+ e^-$ sample is expected to arise from failures of particle identification, typically where one or two high-p_T hadrons interact early and exhibit a shower profile in the calorimeters similar to electrons. Such backgrounds are addressed by the subtraction of the same-sign $Z \rightarrow e^{\pm} e^{\pm}$ candidates. To check whether this procedure is reliable, event samples are studied in which one electron is tagged using the standard requirements, while the second electron satisfies the same criteria except that the requirement on HCAL energy is not satisfied, suggesting that the probe is likely to be a hadron. The numbers of same-sign and opposite-sign pairs satisfying these criteria agree within 5.5%. Treating this as an uncertainty on the background corresponds to an uncertainty of 0.4% in the signal yield, which is taken as the systematic uncertainty on the cross-section. There is no significant variation with y_Z or ϕ^*, so the uncertainty is taken to be the same in all bins and fully correlated between bins.

Physics backgrounds that could give correlated pairs of genuine electron and positron are not necessarily removed by the same-sign subtraction. Production of heavy quark pairs, $c\bar{c}$ or $b\bar{b}$, followed by semileptonic decay could mimic the signal. This contribution is expected to be small, and is found to be negligible using studies of the distribution of the vertex-fit χ^2 for the candidates in data and simulation. The decay $Z \rightarrow \tau^+ \tau^-$ provides a background if both τ-leptons decay to electrons. After the selection, the background from this source is estimated to be 0.15% of the signal using simulated samples, and the prediction is subtracted in each bin of y_Z and ϕ^* as indicated in eq. (3.1) with its statistical uncertainty included in the statistical error. The background arising from production of pairs of gauge bosons, such as $W^+ W^-$ or $W^{\pm} Z$, or of $t\bar{t}$ pairs, is neglected, being well below the 0.1% level, based on expectations from simulation.

5 Results

The measured differential cross-sections as functions of y_Z and ϕ^* are tabulated in tables 2 and 3. The uncertainties in the bins of these distributions are significantly correlated because the luminosity uncertainty and some of the systematic uncertainties are assumed to be common between bins. The correlation matrices between bins of the distributions are presented in tables 4 and 5 of the appendix.

The results are given as Born-level cross-sections, which do not include the effects of final-state radiation. Tables 2 and 3 also include the factors f_{FSR} that permit the measurements to be converted to the particle level after FSR. These are determined using the true momenta of the electrons before and after the generation of FSR in the simulation.

The overall cross-section, obtained by integration of the rapidity distribution, is

$$\sigma(pp \rightarrow Z \rightarrow e^+ e^-) = 93.81 \pm 0.41(\text{stat}) \pm 1.48(\text{syst}) \pm 1.14(\text{lumi}) \text{ pb} \,,$$

where the first uncertainty is statistical, the second includes all experimental systematic effects apart from the contribution from the luminosity, which forms the third uncertainty. When combining the experimental systematic uncertainties, those associated with ϵ_{trig}, and those parts of ϵ_{track}, ϵ_{kin} and ϵ_{PID} arising from the size of the Monte Carlo sample, are treated

y_Z	$d\sigma/dy_Z$ [pb]	f_{FSR}
2.000–2.125	$8.27 \pm 0.37 \pm 0.21 \pm 0.14 \pm 0.10$	0.953 ± 0.003
2.125–2.250	$26.17 \pm 0.61 \pm 0.32 \pm 0.43 \pm 0.32$	0.955 ± 0.002
2.250–2.375	$40.29 \pm 0.72 \pm 0.36 \pm 0.62 \pm 0.49$	0.959 ± 0.001
2.375–2.500	$52.16 \pm 0.80 \pm 0.39 \pm 0.81 \pm 0.64$	0.960 ± 0.001
2.500–2.625	$61.92 \pm 0.86 \pm 0.40 \pm 1.01 \pm 0.77$	0.958 ± 0.001
2.625–2.750	$72.32 \pm 0.93 \pm 0.45 \pm 1.10 \pm 0.88$	0.958 ± 0.001
2.750–2.875	$76.29 \pm 0.98 \pm 0.47 \pm 1.16 \pm 0.93$	0.956 ± 0.001
2.875–3.000	$77.67 \pm 0.99 \pm 0.48 \pm 1.18 \pm 0.95$	0.952 ± 0.001
3.000–3.125	$77.72 \pm 1.03 \pm 0.51 \pm 1.18 \pm 0.95$	0.952 ± 0.001
3.125–3.250	$69.58 \pm 1.02 \pm 0.50 \pm 1.06 \pm 0.85$	0.949 ± 0.001
3.250–3.375	$62.03 \pm 1.01 \pm 0.51 \pm 0.96 \pm 0.76$	0.950 ± 0.001
3.375–3.500	$46.26 \pm 0.92 \pm 0.46 \pm 0.71 \pm 0.56$	0.949 ± 0.001
3.500–3.625	$33.49 \pm 0.84 \pm 0.41 \pm 0.53 \pm 0.41$	0.947 ± 0.002
3.625–3.750	$22.81 \pm 0.74 \pm 0.37 \pm 0.36 \pm 0.28$	0.951 ± 0.002
3.750–3.875	$13.56 \pm 0.64 \pm 0.33 \pm 0.28 \pm 0.17$	0.946 ± 0.002
3.875–4.000	$6.28 \pm 0.57 \pm 0.28 \pm 0.13 \pm 0.08$	0.939 ± 0.004
4.000–4.250	$1.85 \pm 0.33 \pm 0.16 \pm 0.04 \pm 0.02$	0.928 ± 0.005

Table 2. Differential cross-section for $Z \to e^+e^-$ as a function of Z-boson rapidity. The first error is statistical, the second the uncorrelated experimental systematic, the third the correlated experimental systematic and the last error is the uncertainty in luminosity. The cross-sections are at the Born level, *i.e.* before FSR. The rightmost column gives values of the additional factor, f_{FSR}, by which the results should be multiplied in order to give the cross-sections after FSR.

as uncorrelated between bins and therefore combined quadratically; other contributions are treated as fully correlated, as is the luminosity uncertainty, and combined linearly.

The measured cross-section is compared in figure 3 with next-to-next-to-leading order (NNLO; $\mathcal{O}(\alpha_s^2)$) QCD predictions, based on FEWZ version 3.1.b2 [14] using five different PDF sets, MSTW08 [15], CTEQ10 [16], ABM12 [17], NNPDF23 [18] and NNPDF30 [19]. Of these, MSTW08 and CTEQ10 predate the start of LHC data-taking, while ABM12 and NNPDF have included some LHC measurements in their analyses. The uncertainties in the predictions include the effect of varying the renormalisation and factorisation scales by factors of two around the nominal values (set to the Z mass), combined in quadrature with the PDF uncertainties evaluated at 68% confidence level. All predictions are in good agreement with the data.

The differential distribution with respect to y_Z is presented in figure 4 (left) and compared with the NNLO calculations based on FEWZ, all of which are compatible with the integrated cross-section, and model the rapidity distribution as well. In comparing the shapes of the differential cross-sections with theoretical predictions it can be beneficial to normalise them to the integrated cross-section in the acceptance, since most of the correlated systematic uncertainties in the data cancel. This is useful when comparing with

ϕ^*	$d\sigma/d\phi^*$ [pb]						f_{FSR}
0.00–0.01	$996 \pm$	13	$\pm$ 7	$\pm$ 15	$\pm$ 12		0.954 ± 0.001
0.01–0.02	$933 \pm$	13	$\pm$ 7	$\pm$ 14	$\pm$ 11		0.955 ± 0.001
0.02–0.03	$851 \pm$	12	$\pm$ 6	$\pm$ 13	$\pm$ 10		0.954 ± 0.001
0.03–0.05	$664 \pm$	8	$\pm$ 4	$\pm$ 10	$\pm$ 8		0.954 ± 0.001
0.05–0.07	$505 \pm$	7	$\pm$ 3	$\pm$ 7	$\pm$ 6		0.953 ± 0.001
0.07–0.10	$346 \pm$	5	$\pm$ 2	$\pm$ 5	$\pm$ 4		0.952 ± 0.001
0.10–0.15	$221.5 \pm$	2.9	$\pm$ 1.4	$\pm$ 3.4	$\pm$ 2.7		0.953 ± 0.001
0.15–0.20	$126.9 \pm$	2.2	$\pm$ 1.1	$\pm$ 2.0	$\pm$ 1.6		0.952 ± 0.001
0.20–0.30	$65.8 \pm$	1.1	$\pm$ 0.5	$\pm$ 1.0	$\pm$ 0.8		0.949 ± 0.001
0.30–0.40	$32.2 \pm$	0.8	$\pm$ 0.4	$\pm$ 0.5	$\pm$ 0.4		0.951 ± 0.002
0.40–0.60	$13.86 \pm$	0.36	$\pm$ 0.17	$\pm$ 0.22	$\pm$ 0.17		0.951 ± 0.002
0.60–0.80	$5.63 \pm$	0.23	$\pm$ 0.11	$\pm$ 0.09	$\pm$ 0.07		0.955 ± 0.003
0.80–1.20	$1.64 \pm$	0.09	$\pm$ 0.04	$\pm$ 0.03	$\pm$ 0.02		0.957 ± 0.003
1.20–2.00	$0.334 \pm$	0.026	$\pm$ 0.013	$\pm$ 0.006	$\pm$ 0.004		0.957 ± 0.005
2.00–4.00	$0.031 \pm$	0.006	$\pm$ 0.002	$\pm$ 0.001	$\pm$ 0.001		0.966 ± 0.007

Table 3. Differential cross-section for $Z \to e^+e^-$ as a function of ϕ^*. The first error is statistical, the second the uncorrelated experimental systematic, the third the correlated experimental systematic and the last error is the uncertainty in luminosity. The cross-sections are at the Born level, *i.e.* before FSR. The rightmost column gives values of the additional factor, f_{FSR}, by which the results should be multiplied in order to give the cross-sections after FSR.
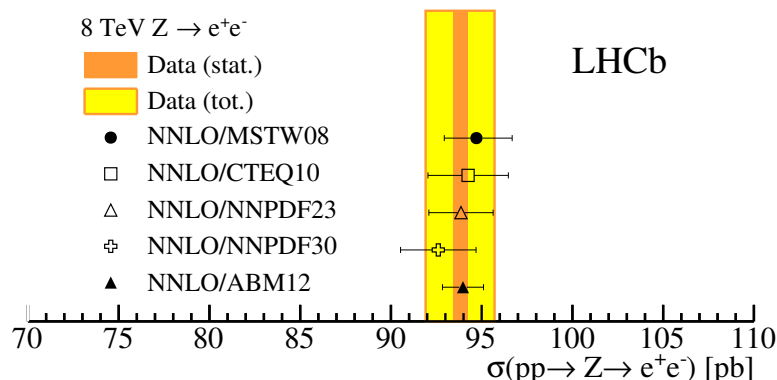

Figure 3. Measured cross-section for $Z \to e^+e^-$ shown as the shaded band, with the inner (orange) band indicating the statistical error and the outer (yellow) band the total uncertainty. For comparison, the NNLO predictions of FEWZ are shown using five different sets of PDFs. The uncertainties on these predictions include the PDF uncertainties and the variation of the factorisation and normalisation scales, as well as the errors arising from numerical integration.

models based on LO or NLO calculations, which may predict the integrated cross-section well. The normalised differential distribution with respect to y_Z is presented in figure 4 (right) and compared with calculations that partially take account of higher-order effects. A
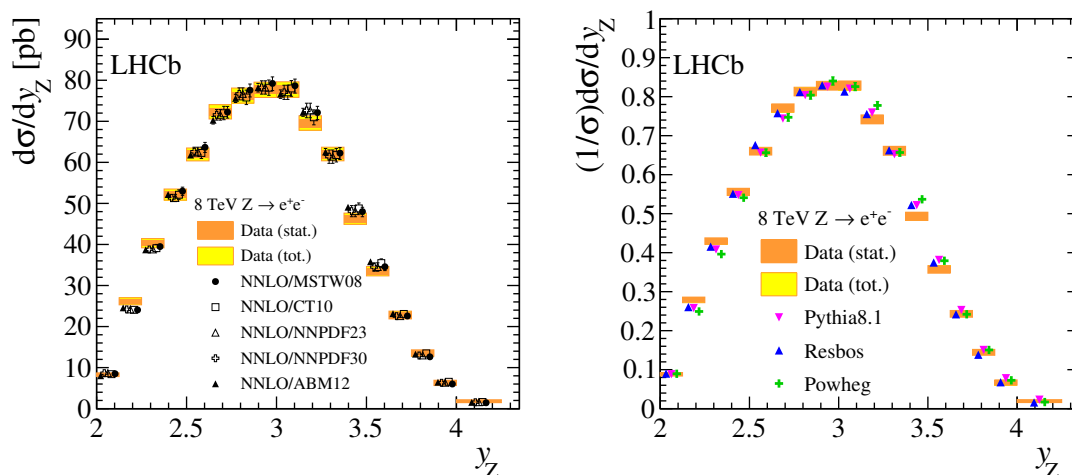
Figure 4. (left) Differential cross-section $d\sigma/dy_Z$ and (right) normalised differential cross-section $(1/\sigma)d\sigma/dy_Z$ as a function of y_Z. The measured data are shown as the shaded bands, with the inner (orange) bands indicating the statistical error and the outer (yellow) bands the total uncertainty. For comparison, the NNLO predictions of FEWZ using five different sets of PDFs are shown on the left-hand plot. The same data are compared with leading log calculations in the right-hand plot. To aid clarity, small horizontal displacements are applied to some of the predictions.

QCD calculation that takes multiple soft gluon emissions into account through resummation is provided by RESBOS [20, 21].[4] Alternatively, POWHEG [22, 23] provides a framework whereby a NLO ($\mathcal{O}(\alpha_s)$) calculation can be interfaced to a parton shower model such as PYTHIA, which can approximate higher-order effects. The parton shower model of PYTHIA 8.1 [7, 8] is also compared with the data. All approaches reproduce the main features of the rapidity distribution.

Studies at 7 TeV [4] showed that the NNLO calculations based on FEWZ fail to model the ϕ^* distribution. It is expected that the ϕ^* distribution, like that of p_T, is significantly affected by multiple soft gluon emissions, which are not sufficiently accounted for in fixed-order calculations. The present data exhibit the same behaviour, and this comparison is not shown. The normalised distribution with respect to ϕ^* is therefore presented in figure 5 (left) and compared with the RESBOS, POWHEG and PYTHIA 8.1 calculations. These all model the data reasonably well, especially at lower ϕ^* where differences are typically up to the 10% level, while larger discrepancies are seen for $\phi^* > 1$. To show this more clearly, the ratios between the calculations that include higher orders and the data for the ϕ^* distribution are also shown in figure 5 (right). The data tend to fall between the different models, indicating no clear preference for any of them.

6   Summary

A measurement of the cross-section for Z-boson production in the forward region of pp collisions at 8 TeV centre-of-mass energy is presented. The measurement, using an integrated

---

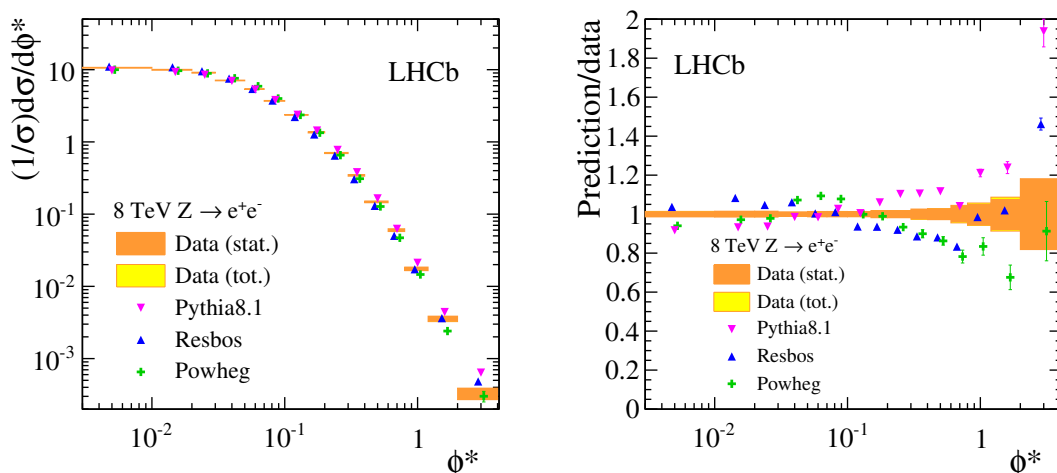[4]The P branch of RESBOS is used with grids for LHC at $\sqrt{s} = 8$ TeV based on CTEQ6.6.

Figure 5. (left) Normalised differential cross-section $(1/\sigma)\mathrm{d}\sigma/\mathrm{d}\phi^*$ as a function of ϕ^*. The measured data are shown as the shaded bands, with the inner (orange) bands indicating the statistical error and the outer (yellow) bands the total uncertainty. For comparison, the predictions of the leading-log calculations described in the text are shown. (right) The same data and predictions normalised to the measurement in data, so that the measurements are shown as the shaded bands at unity. To aid clarity, small horizontal displacements are applied to some of the predictions.

luminosity of 2.0 fb^{-1} recorded using the LHCb detector, is based on the Z $\rightarrow$ e$^+$e$^-$ decay. The acceptance is defined by the requirements $2.0 < \eta < 4.5$ and $p_\mathrm{T} > 20$ GeV for the leptons while their invariant mass is required to lie in the range 60–120 GeV. The cross-section is determined to be

$$\sigma(\mathrm{pp} \rightarrow \mathrm{Z} \rightarrow \mathrm{e}^+\mathrm{e}^-) = 93.81 \pm 0.41(\mathrm{stat}) \pm 1.48(\mathrm{syst}) \pm 1.14(\mathrm{lumi}) \text{ pb},$$

where the first uncertainty is statistical and the second reflects all systematic uncertainties apart from that associated with the luminosity, which is given as the third uncertainty. Differential cross-sections are also presented as functions of the Z-boson rapidity, and the angular variable ϕ^*. The rapidity distribution is well modelled by NNLO calculations, and is compared with several recent sets of parton distribution functions. A reasonable description of the ϕ^* distribution requires the use of calculations that implement approximations of higher orders, either through resummation or using parton shower techniques.

Acknowledgments

A Correlation matrices

Bin index	1	2	3	4	5	6	7	8	9	10	11	12	13	14	15	16	17
1	1.00																
2	0.23	1.00															
3	0.26	0.43	1.00														
4	0.22	0.36	0.41	1.00													
5	0.30	0.49	0.56	0.47	1.00												
6	0.30	0.50	0.56	0.47	0.64	1.00											
7	0.30	0.50	0.57	0.47	0.65	0.65	1.00										
8	0.30	0.50	0.57	0.47	0.65	0.65	0.65	1.00									
9	0.30	0.49	0.56	0.47	0.64	0.64	0.65	0.64	1.00								
10	0.28	0.47	0.54	0.45	0.61	0.62	0.62	0.62	0.61	1.00							
11	0.27	0.45	0.51	0.43	0.58	0.59	0.59	0.59	0.58	0.56	1.00						
12	0.25	0.41	0.46	0.39	0.53	0.53	0.54	0.54	0.53	0.51	0.49	1.00					
13	0.22	0.36	0.41	0.34	0.47	0.47	0.47	0.47	0.47	0.45	0.43	0.39	1.00				
14	0.18	0.30	0.34	0.28	0.39	0.39	0.39	0.39	0.39	0.37	0.35	0.32	0.28	1.00			
15	0.15	0.26	0.29	0.24	0.33	0.33	0.33	0.33	0.33	0.32	0.30	0.27	0.24	0.20	1.00		
16	0.09	0.14	0.16	0.14	0.18	0.19	0.19	0.19	0.18	0.18	0.17	0.15	0.13	0.11	0.10	1.00	
17	0.04	0.07	0.08	0.07	0.10	0.10	0.10	0.10	0.10	0.09	0.09	0.08	0.07	0.06	0.05	0.03	1.00

Table 4. Correlation matrix between bins of y_Z. The bin numbering follows the same sequence as table 2.

Bin index	1	2	3	4	5	6	7	8	9	10	11	12	13	14	15
1	1.00														
2	0.63	1.00													
3	0.62	0.61	1.00												
4	0.82	0.80	0.79	1.00											
5	0.64	0.63	0.62	0.82	1.00										
6	0.64	0.63	0.62	0.82	0.64	1.00									
7	0.65	0.64	0.63	0.83	0.65	0.65	1.00								
8	0.58	0.57	0.56	0.74	0.58	0.58	0.59	1.00							
9	0.58	0.58	0.57	0.75	0.59	0.59	0.59	0.53	1.00						
10	0.48	0.48	0.47	0.62	0.49	0.49	0.49	0.44	0.44	1.00					
11	0.46	0.46	0.45	0.59	0.47	0.47	0.47	0.42	0.43	0.35	1.00				
12	0.35	0.34	0.34	0.44	0.35	0.35	0.35	0.31	0.32	0.26	0.25	1.00			
13	0.30	0.30	0.30	0.39	0.31	0.31	0.31	0.28	0.28	0.23	0.22	0.16	1.00		
14	0.22	0.22	0.21	0.28	0.22	0.22	0.22	0.20	0.20	0.17	0.16	0.12	0.10	1.00	
15	0.10	0.10	0.10	0.13	0.10	0.10	0.10	0.09	0.09	0.08	0.07	0.06	0.05	0.04	1.00

Table 5. Correlation matrix between bins of ϕ^*. The bin numbering follows the same sequence as table 3.

References

[1] LHCb collaboration, *The LHCb Detector at the LHC*, 2008 *JINST* **3** S08005 [ɪɴSPIRE].

[2] R.S. Thorne, A.D. Martin, W.J. Stirling and G. Watt, *Parton Distributions and QCD at LHCb*, `arXiv:0808.1847` [ɪɴSPIRE].

[3] LHCb collaboration, *Inclusive W and Z production in the forward region at $\sqrt{s} = 7$ TeV*, *JHEP* **06** (2012) 058 [`arXiv:1204.1620`] [ɪɴSPIRE].

[4] LHCb collaboration, *Measurement of the cross-section for $Z \to e^+e^-$ production in pp collisions at $\sqrt{s} = 7$ TeV*, *JHEP* **02** (2013) 106 [`arXiv:1212.4620`] [ɪɴSPIRE].

[5] A. Banfi, S. Redford, M. Vesterinen, P. Waller and T.R. Wyatt, *Optimisation of variables for studying dilepton transverse momentum distributions at hadron colliders*, *Eur. Phys. J.* **C 71** (2011) 1600 [`arXiv:1009.1580`] [ɪɴSPIRE].

[6] LHCb collaboration, *LHCb Detector Performance*, *Int. J. Mod. Phys.* **A 30** (2015) 1530022 [`arXiv:1412.6352`] [ɪɴSPIRE].

[7] T. Sjöstrand, S. Mrenna and P.Z. Skands, *PYTHIA 6.4 Physics and Manual*, *JHEP* **05** (2006) 026 [`hep-ph/0603175`] [ɪɴSPIRE].

[8] T. Sjöstrand, S. Mrenna and P.Z. Skands, *A Brief Introduction to PYTHIA 8.1*, *Comput. Phys. Commun.* **178** (2008) 852 [`arXiv:0710.3820`] [ɪɴSPIRE].

[9] I. Belyaev et al., *Handling of the generation of primary events in Gauss, the LHCb simulation framework*, *IEEE Nucl. Sci. Symp. Conf. Rec.* (2010) 1155.

[10] Geant4 collaboration, J. Allison et al., *Geant4 developments and applications*, *IEEE Trans. Nucl. Sci.* **53** (2006) 270.

[11] Geant4 collaboration, S. Agostinelli et al., *Geant4: A Simulation toolkit*, *Nucl. Instrum. Meth.* **A 506** (2003) 250 [ɪɴSPIRE].

[12] M. Clemencic et al., *The LHCb simulation application, Gauss: Design, evolution and experience*, *J. Phys. Conf. Ser.* **331** (2011) 032023 [ɪɴSPIRE].

[13] LHCb collaboration, *Precision luminosity measurements at LHCb*, 2014 *JINST* **9** P12005 [`arXiv:1410.0149`] [ɪɴSPIRE].

[14] Y. Li and F. Petriello, *Combining QCD and electroweak corrections to dilepton production in FEWZ*, *Phys. Rev.* **D 86** (2012) 094034 [`arXiv:1208.5967`] [ɪɴSPIRE].

[15] A.D. Martin, W.J. Stirling, R.S. Thorne and G. Watt, *Parton distributions for the LHC*, *Eur. Phys. J.* **C 63** (2009) 189 [`arXiv:0901.0002`] [ɪɴSPIRE].

[16] H.-L. Lai et al., *New parton distributions for collider physics*, *Phys. Rev.* **D 82** (2010) 074024 [`arXiv:1007.2241`] [ɪɴSPIRE].

[17] S. Alekhin, J. Bluemlein and S. Moch, *The ABM parton distributions tuned to LHC data*, *Phys. Rev.* **D 89** (2014) 054028 [`arXiv:1310.3059`] [ɪɴSPIRE].

[18] R.D. Ball et al., *Parton distributions with LHC data*, *Nucl. Phys.* **B 867** (2013) 244 [`arXiv:1207.1303`] [ɪɴSPIRE].

[19] NNPDF collaboration, R.D. Ball et al., *Parton distributions for the LHC Run II*, *JHEP* **04** (2015) 040 [`arXiv:1410.8849`] [INSPIRE].

[20] G.A. Ladinsky and C.P. Yuan, *The Nonperturbative regime in QCD resummation for gauge boson production at hadron colliders*, *Phys. Rev.* **D 50** (1994) 4239 [`hep-ph/9311341`] [INSPIRE].

[21] C. Balázs and C.P. Yuan, *Soft gluon effects on lepton pairs at hadron colliders*, *Phys. Rev.* **D 56** (1997) 5558 [`hep-ph/9704258`] [INSPIRE].

[22] S. Alioli, P. Nason, C. Oleari and E. Re, *NLO vector-boson production matched with shower in POWHEG*, *JHEP* **07** (2008) 060 [`arXiv:0805.4802`] [INSPIRE].

[23] S. Alioli, P. Nason, C. Oleari and E. Re, *Vector boson plus one jet production in POWHEG*, *JHEP* **01** (2011) 095 [`arXiv:1009.5594`] [INSPIRE].

The LHCb collaboration

R. Aaij[41], B. Adeva[37], M. Adinolfi[46], A. Affolder[52], Z. Ajaltouni[5], S. Akar[6], J. Albrecht[9],
F. Alessio[38], M. Alexander[51], S. Ali[41], G. Alkhazov[30], P. Alvarez Cartelle[53], A.A. Alves Jr[57],
S. Amato[2], S. Amerio[22], Y. Amhis[7], L. An[3], L. Anderlini[17,g], J. Anderson[40], M. Andreotti[16,f],
J.E. Andrews[58], R.B. Appleby[54], O. Aquines Gutierrez[10], F. Archilli[38], A. Artamonov[35],
M. Artuso[59], E. Aslanides[6], G. Auriemma[25,n], M. Baalouch[5], S. Bachmann[11], J.J. Back[48],
A. Badalov[36], C. Baesso[60], W. Baldini[16,38], R.J. Barlow[54], C. Barschel[38], S. Barsuk[7], W. Barter[38],
V. Batozskaya[28], V. Battista[39], A. Bay[39], L. Beaucourt[4], J. Beddow[51], F. Bedeschi[23], I. Bediaga[1],
I. Belyaev[31], E. Ben-Haim[8], G. Bencivenni[18], S. Benson[38], J. Benton[46], A. Berezhnoy[32],
R. Bernet[40], A. Bertolin[22], M.-O. Bettler[38], M. van Beuzekom[41], A. Bien[11], S. Bifani[45], T. Bird[54],
A. Bizzeti[17,i], T. Blake[48], F. Blanc[39], J. Blouw[10], S. Blusk[59], V. Bocci[25], A. Bondar[34],
N. Bondar[30,38], W. Bonivento[15], S. Borghi[54], A. Borgia[59], M. Borsato[7], T.J.V. Bowcock[52],
E. Bowen[40], C. Bozzi[16], S. Braun[11], D. Brett[54], M. Britsch[10], T. Britton[59], J. Brodzicka[54],
N.H. Brook[46], A. Bursche[40], J. Buytaert[38], S. Cadeddu[15], R. Calabrese[16,f], M. Calvi[20,k],
M. Calvo Gomez[36,p], P. Campana[18], D. Campora Perez[38], L. Capriotti[54], A. Carbone[14,d],
G. Carboni[24,l], R. Cardinale[19,j], A. Cardini[15], P. Carniti[20], L. Carson[50], K. Carvalho Akiba[2,38],
R. Casanova Mohr[36], G. Casse[52], L. Cassina[20,k], L. Castillo Garcia[38], M. Cattaneo[38], Ch. Cauet[9],
G. Cavallero[19], R. Cenci[23,t], M. Charles[8], Ph. Charpentier[38], M. Chefdeville[4], S. Chen[54],
S.-F. Cheung[55], N. Chiapolini[40], M. Chrzaszcz[40,26], X. Cid Vidal[38], G. Ciezarek[41], P.E.L. Clarke[50],
M. Clemencic[38], H.V. Cliff[47], J. Closier[38], V. Coco[38], J. Cogan[6], E. Cogneras[5], V. Cogoni[15,e],
L. Cojocariu[29], G. Collazuol[22], P. Collins[38], A. Comerma-Montells[11], A. Contu[15,38], A. Cook[46],
M. Coombes[46], S. Coquereau[8], G. Corti[38], M. Corvo[16,f], I. Counts[56], B. Couturier[38],
G.A. Cowan[50], D.C. Craik[48], A.C. Crocombe[48], M. Cruz Torres[60], S. Cunliffe[53], R. Currie[53],
C. D'Ambrosio[38], J. Dalseno[46], P.N.Y. David[41], A. Davis[57], K. De Bruyn[41], S. De Capua[54],
M. De Cian[11], J.M. De Miranda[1], L. De Paula[2], W. De Silva[57], P. De Simone[18], C.-T. Dean[51],
D. Decamp[4], M. Deckenhoff[9], L. Del Buono[8], N. Déléage[4], D. Derkach[55], O. Deschamps[5],
F. Dettori[38], B. Dey[40], A. Di Canto[38], F. Di Ruscio[24], H. Dijkstra[38], S. Donleavy[52], F. Dordei[11],
M. Dorigo[39], A. Dosil Suárez[37], D. Dossett[48], A. Dovbnya[43], K. Dreimanis[52], G. Dujany[54],
F. Dupertuis[39], P. Durante[38], R. Dzhelyadin[35], A. Dziurda[26], A. Dzyuba[30], S. Easo[49,38],
U. Egede[53], V. Egorychev[31], S. Eidelman[34], S. Eisenhardt[50], U. Eitschberger[9], R. Ekelhof[9],
L. Eklund[51], I. El Rifai[5], Ch. Elsasser[40], S. Ely[59], S. Esen[11], H.M. Evans[47], T. Evans[55],
A. Falabella[14], C. Färber[11], C. Farinelli[41], N. Farley[45], S. Farry[52], R. Fay[52], D. Ferguson[50],
V. Fernandez Albor[37], F. Ferreira Rodrigues[1], M. Ferro-Luzzi[38], S. Filippov[33], M. Fiore[16,38,f],
M. Fiorini[16,f], M. Firlej[27], C. Fitzpatrick[39], T. Fiutowski[27], P. Fol[53], M. Fontana[10],
F. Fontanelli[19,j], R. Forty[38], O. Francisco[2], M. Frank[38], C. Frei[38], M. Frosini[17], J. Fu[21,38],
E. Furfaro[24,l], A. Gallas Torreira[37], D. Galli[14,d], S. Gallorini[22,38], S. Gambetta[19,j], M. Gandelman[2],
P. Gandini[55], Y. Gao[3], J. García Pardiñas[37], J. Garofoli[59], J. Garra Tico[47], L. Garrido[36],
D. Gascon[36], C. Gaspar[38], U. Gastaldi[16], R. Gauld[55], L. Gavardi[9], G. Gazzoni[5], A. Geraci[21,v],
E. Gersabeck[11], M. Gersabeck[54], T. Gershon[48], Ph. Ghez[4], A. Gianelle[22], S. Gianì[39], V. Gibson[47],
L. Giubega[29], V.V. Gligorov[38], C. Göbel[60], D. Golubkov[31], A. Golutvin[53,31,38], A. Gomes[1,a],
C. Gotti[20,k], M. Grabalosa Gándara[5], R. Graciani Diaz[36], L.A. Granado Cardoso[38], E. Graugés[36],
E. Graverini[40], G. Graziani[17], A. Grecu[29], E. Greening[55], S. Gregson[47], P. Griffith[45], L. Grillo[11],
O. Grünberg[63], B. Gui[59], E. Gushchin[33], Yu. Guz[35,38], T. Gys[38], C. Hadjivasiliou[59], G. Haefeli[39],
C. Haen[38], S.C. Haines[47], S. Hall[53], B. Hamilton[58], T. Hampson[46], X. Han[11],
S. Hansmann-Menzemer[11], N. Harnew[55], S.T. Harnew[46], J. Harrison[54], J. He[38], T. Head[39],
V. Heijne[41], K. Hennessy[52], P. Henrard[5], L. Henry[8], J.A. Hernando Morata[37], E. van Herwijnen[38],
M. Heß[63], A. Hicheur[2], D. Hill[55], M. Hoballah[5], C. Hombach[54], W. Hulsbergen[41], T. Humair[53],

N. Hussain[55], D. Hutchcroft[52], D. Hynds[51], M. Idzik[27], P. Ilten[56], R. Jacobsson[38], A. Jaeger[11],
J. Jalocha[55], E. Jans[41], A. Jawahery[58], F. Jing[3], M. John[55], D. Johnson[38], C.R. Jones[47],
C. Joram[38], B. Jost[38], N. Jurik[59], S. Kandybei[43], W. Kanso[6], M. Karacson[38], T.M. Karbach[38],
S. Karodia[51], M. Kelsey[59], I.R. Kenyon[45], M. Kenzie[38], T. Ketel[42], B. Khanji[20,38,k],
C. Khurewathanakul[39], S. Klaver[54], K. Klimaszewski[28], O. Kochebina[7], M. Kolpin[11], I. Komarov[39],
R.F. Koopman[42], P. Koppenburg[41,38], M. Korolev[32], L. Kravchuk[33], K. Kreplin[11], M. Kreps[48],
G. Krocker[11], P. Krokovny[34], F. Kruse[9], W. Kucewicz[26,o], M. Kucharczyk[26], V. Kudryavtsev[34],
K. Kurek[28], T. Kvaratskheliya[31], V.N. La Thi[39], D. Lacarrere[38], G. Lafferty[54], A. Lai[15],
D. Lambert[50], R.W. Lambert[42], G. Lanfranchi[18], C. Langenbruch[48], B. Langhans[38], T. Latham[48],
C. Lazzeroni[45], R. Le Gac[6], J. van Leerdam[41], J.-P. Lees[4], R. Lefèvre[5], A. Leflat[32], J. Lefrançois[7],
O. Leroy[6], T. Lesiak[26], B. Leverington[11], Y. Li[7], T. Likhomanenko[64], M. Liles[52], R. Lindner[38],
C. Linn[38], F. Lionetto[40], B. Liu[15], S. Lohn[38], I. Longstaff[51], J.H. Lopes[2], P. Lowdon[40],
D. Lucchesi[22,r], H. Luo[50], A. Lupato[22], E. Luppi[16,f], O. Lupton[55], F. Machefert[7],
I.V. Machikhiliyan[31], F. Maciuc[29], O. Maev[30], S. Malde[55], A. Malinin[64], G. Manca[15,e],
G. Mancinelli[6], P Manning[59], A. Mapelli[38], J. Maratas[5], J.F. Marchand[4], U. Marconi[14],
C. Marin Benito[36], P. Marino[23,38,t], R. Märki[39], J. Marks[11], G. Martellotti[25], M. Martinelli[39],
D. Martinez Santos[42], F. Martinez Vidal[66], D. Martins Tostes[2], A. Massafferri[1], R. Matev[38],
Z. Mathe[38], C. Matteuzzi[20], A Mauri[40], B. Maurin[39], A. Mazurov[45], M. McCann[53], J. McCarthy[45],
A. McNab[54], R. McNulty[12], B. McSkelly[52], B. Meadows[57], F. Meier[9], M. Meissner[11], M. Merk[41],
D.A. Milanes[62], M.-N. Minard[4], J. Molina Rodriguez[60], S. Monteil[5], M. Morandin[22],
P. Morawski[27], A. Mordà[6], M.J. Morello[23,t], J. Moron[27], A.-B. Morris[50], R. Mountain[59],
F. Muheim[50], K. Müller[40], M. Mussini[14], B. Muster[39], P. Naik[46], T. Nakada[39], R. Nandakumar[49],
I. Nasteva[2], M. Needham[50], N. Neri[21], S. Neubert[11], N. Neufeld[38], M. Neuner[11], A.D. Nguyen[39],
T.D. Nguyen[39], C. Nguyen-Mau[39,q], V. Niess[5], R. Niet[9], N. Nikitin[32], T. Nikodem[11],
A. Novoselov[35], D.P. O'Hanlon[48], A. Oblakowska-Mucha[27], V. Obraztsov[35], S. Ogilvy[51],
O. Okhrimenko[44], R. Oldeman[15,e], C.J.G. Onderwater[67], B. Osorio Rodrigues[1],
J.M. Otalora Goicochea[2], A. Otto[38], P. Owen[53], A. Oyanguren[66], A. Palano[13,c], F. Palombo[21,u],
M. Palutan[18], J. Panman[38], A. Papanestis[49], M. Pappagallo[51], L.L. Pappalardo[16,f], C. Parkes[54],
G. Passaleva[17], G.D. Patel[52], M. Patel[53], C. Patrignani[19,j], A. Pearce[54,49], A. Pellegrino[41],
G. Penso[25,m], M. Pepe Altarelli[38], S. Perazzini[14,d], P. Perret[5], L. Pescatore[45], E. Pesen[68],
K. Petridis[46], A. Petrolini[19,j], E. Picatoste Olloqui[36], B. Pietrzyk[4], T. Pilar[48], D. Pinci[25],
A. Pistone[19], S. Playfer[50], M. Plo Casasus[37], T. Poikela[38], F. Polci[8], A. Poluektov[48,34],
I. Polyakov[31], E. Polycarpo[2], A. Popov[35], D. Popov[10], B. Popovici[29], C. Potterat[2], E. Price[46],
J.D. Price[52], J. Prisciandaro[39], A. Pritchard[52], C. Prouve[46], V. Pugatch[44], A. Puig Navarro[39],
G. Punzi[23,s], W. Qian[4], R Quagliani[7,46], B. Rachwal[26], J.H. Rademacker[46],
B. Rakotomiaramanana[39], M. Rama[23], M.S. Rangel[2], I. Raniuk[43], N. Rauschmayr[38], G. Raven[42],
F. Redi[53], S. Reichert[54], M.M. Reid[48], A.C. dos Reis[1], S. Ricciardi[49], S. Richards[46], M. Rihl[38],
K. Rinnert[52], V. Rives Molina[36], P. Robbe[7,38], A.B. Rodrigues[1], E. Rodrigues[54],
J.A. Rodriguez Lopez[62], P. Rodriguez Perez[54], S. Roiser[38], V. Romanovsky[35], A. Romero Vidal[37],
M. Rotondo[22], J. Rouvinet[39], T. Ruf[38], H. Ruiz[36], P. Ruiz Valls[66], J.J. Saborido Silva[37],
N. Sagidova[30], P. Sail[51], B. Saitta[15,e], V. Salustino Guimaraes[2], C. Sanchez Mayordomo[66],
B. Sanmartin Sedes[37], R. Santacesaria[25], C. Santamarina Rios[37], E. Santovetti[24,l], A. Sarti[18,m],
C. Satriano[25,n], A. Satta[24], D.M. Saunders[46], D. Savrina[31,32], M. Schiller[38], H. Schindler[38],
M. Schlupp[9], M. Schmelling[10], B. Schmidt[38], O. Schneider[39], A. Schopper[38], M.-H. Schune[7],
R. Schwemmer[38], B. Sciascia[18], A. Sciubba[25,m], A. Semennikov[31], I. Sepp[53], N. Serra[40],
J. Serrano[6], L. Sestini[22], P. Seyfert[11], M. Shapkin[35], I. Shapoval[16,43,f], Y. Shcheglov[30], T. Shears[52],
L. Shekhtman[34], V. Shevchenko[64], A. Shires[9], R. Silva Coutinho[48], G. Simi[22], M. Sirendi[47],
N. Skidmore[46], I. Skillicorn[51], T. Skwarnicki[59], N.A. Smith[52], E. Smith[55,49], E. Smith[53], J. Smith[47],

M. Smith[54], H. Snoek[41], M.D. Sokoloff[57,38], F.J.P. Soler[51], F. Soomro[39], D. Souza[46],
B. Souza De Paula[2], B. Spaan[9], P. Spradlin[51], S. Sridharan[38], F. Stagni[38], M. Stahl[11], S. Stahl[38],
O. Steinkamp[40], O. Stenyakin[35], F Sterpka[59], S. Stevenson[55], S. Stoica[29], S. Stone[59], B. Storaci[40],
S. Stracka[23,t], M. Straticiuc[29], U. Straumann[40], R. Stroili[22], L. Sun[57], W. Sutcliffe[53],
K. Swientek[27], S. Swientek[9], V. Syropoulos[42], M. Szczekowski[28], P. Szczypka[39,38], T. Szumlak[27],
S. T'Jampens[4], M. Teklishyn[7], G. Tellarini[16,f], F. Teubert[38], C. Thomas[55], E. Thomas[38],
J. van Tilburg[41], V. Tisserand[4], M. Tobin[39], J. Todd[57], S. Tolk[42], L. Tomassetti[16,f], D. Tonelli[38],
S. Topp-Joergensen[55], N. Torr[55], E. Tournefier[4], S. Tourneur[39], K. Trabelsi[39], M.T. Tran[39],
M. Tresch[40], A. Trisovic[38], A. Tsaregorodtsev[6], P. Tsopelas[41], N. Tuning[41,38], M. Ubeda Garcia[38],
A. Ukleja[28], A. Ustyuzhanin[65], U. Uwer[11], C. Vacca[15,e], V. Vagnoni[14], G. Valenti[14], A. Vallier[7],
R. Vazquez Gomez[18], P. Vazquez Regueiro[37], C. Vázquez Sierra[37], S. Vecchi[16], J.J. Velthuis[46],
M. Veltri[17,h], G. Veneziano[39], M. Vesterinen[11], J.V. Viana Barbosa[38], B. Viaud[7], D. Vieira[2],
M. Vieites Diaz[37], X. Vilasis-Cardona[36,p], A. Vollhardt[40], D. Volyanskyy[10], D. Voong[46],
A. Vorobyev[30], V. Vorobyev[34], C. Voß[63], J.A. de Vries[41], R. Waldi[63], C. Wallace[48], R. Wallace[12],
J. Walsh[23], S. Wandernoth[11], J. Wang[59], D.R. Ward[47], N.K. Watson[45], D. Websdale[53],
A. Weiden[40], M. Whitehead[48], D. Wiedner[11], G. Wilkinson[55,38], M. Wilkinson[59], M. Williams[38],
M.P. Williams[45], M. Williams[56], H.W. Wilschut[67], F.F. Wilson[49], J. Wimberley[58], J. Wishahi[9],
W. Wislicki[28], M. Witek[26], G. Wormser[7], S.A. Wotton[47], S. Wright[47], K. Wyllie[38], Y. Xie[61],
Z. Xu[39], Z. Yang[3], X. Yuan[34], O. Yushchenko[35], M. Zangoli[14], M. Zavertyaev[10,b], L. Zhang[3],
Y. Zhang[3], A. Zhelezov[11], A. Zhokhov[31], L. Zhong[3].

1 Centro Brasileiro de Pesquisas Físicas (CBPF), Rio de Janeiro, Brazil
2 Universidade Federal do Rio de Janeiro (UFRJ), Rio de Janeiro, Brazil
3 Center for High Energy Physics, Tsinghua University, Beijing, China
4 LAPP, Université Savoie Mont-Blanc, CNRS/IN2P3, Annecy-Le-Vieux, France
5 Clermont Université, Université Blaise Pascal, CNRS/IN2P3, LPC, Clermont-Ferrand, France
6 CPPM, Aix-Marseille Université, CNRS/IN2P3, Marseille, France
7 LAL, Université Paris-Sud, CNRS/IN2P3, Orsay, France
8 LPNHE, Université Pierre et Marie Curie, Université Paris Diderot, CNRS/IN2P3, Paris, France
9 Fakultät Physik, Technische Universität Dortmund, Dortmund, Germany
10 Max-Planck-Institut für Kernphysik (MPIK), Heidelberg, Germany
11 Physikalisches Institut, Ruprecht-Karls-Universität Heidelberg, Heidelberg, Germany
12 School of Physics, University College Dublin, Dublin, Ireland
13 Sezione INFN di Bari, Bari, Italy
14 Sezione INFN di Bologna, Bologna, Italy
15 Sezione INFN di Cagliari, Cagliari, Italy
16 Sezione INFN di Ferrara, Ferrara, Italy
17 Sezione INFN di Firenze, Firenze, Italy
18 Laboratori Nazionali dell'INFN di Frascati, Frascati, Italy
19 Sezione INFN di Genova, Genova, Italy
20 Sezione INFN di Milano Bicocca, Milano, Italy
21 Sezione INFN di Milano, Milano, Italy
22 Sezione INFN di Padova, Padova, Italy
23 Sezione INFN di Pisa, Pisa, Italy
24 Sezione INFN di Roma Tor Vergata, Roma, Italy
25 Sezione INFN di Roma La Sapienza, Roma, Italy
26 Henryk Niewodniczanski Institute of Nuclear Physics Polish Academy of Sciences, Kraków, Poland
27 AGH - University of Science and Technology, Faculty of Physics and Applied Computer Science, Kraków, Poland
28 National Center for Nuclear Research (NCBJ), Warsaw, Poland
29 Horia Hulubei National Institute of Physics and Nuclear Engineering, Bucharest-Magurele, Romania

30   *Petersburg Nuclear Physics Institute (PNPI), Gatchina, Russia*

31   *Institute of Theoretical and Experimental Physics (ITEP), Moscow, Russia*

32   *Institute of Nuclear Physics, Moscow State University (SINP MSU), Moscow, Russia*

33   *Institute for Nuclear Research of the Russian Academy of Sciences (INR RAN), Moscow, Russia*

34   *Budker Institute of Nuclear Physics (SB RAS) and Novosibirsk State University, Novosibirsk, Russia*

35   *Institute for High Energy Physics (IHEP), Protvino, Russia*

36   *Universitat de Barcelona, Barcelona, Spain*

37   *Universidad de Santiago de Compostela, Santiago de Compostela, Spain*

38   *European Organization for Nuclear Research (CERN), Geneva, Switzerland*

39   *Ecole Polytechnique Fédérale de Lausanne (EPFL), Lausanne, Switzerland*

40   *Physik-Institut, Universität Zürich, Zürich, Switzerland*

41   *Nikhef National Institute for Subatomic Physics, Amsterdam, The Netherlands*

42   *Nikhef National Institute for Subatomic Physics and VU University Amsterdam, Amsterdam, The Netherlands*

43   *NSC Kharkiv Institute of Physics and Technology (NSC KIPT), Kharkiv, Ukraine*

44   *Institute for Nuclear Research of the National Academy of Sciences (KINR), Kyiv, Ukraine*

45   *University of Birmingham, Birmingham, United Kingdom*

46   *H.H. Wills Physics Laboratory, University of Bristol, Bristol, United Kingdom*

47   *Cavendish Laboratory, University of Cambridge, Cambridge, United Kingdom*

48   *Department of Physics, University of Warwick, Coventry, United Kingdom*

49   *STFC Rutherford Appleton Laboratory, Didcot, United Kingdom*

50   *School of Physics and Astronomy, University of Edinburgh, Edinburgh, United Kingdom*

51   *School of Physics and Astronomy, University of Glasgow, Glasgow, United Kingdom*

52   *Oliver Lodge Laboratory, University of Liverpool, Liverpool, United Kingdom*

53   *Imperial College London, London, United Kingdom*

54   *School of Physics and Astronomy, University of Manchester, Manchester, United Kingdom*

55   *Department of Physics, University of Oxford, Oxford, United Kingdom*

56   *Massachusetts Institute of Technology, Cambridge, MA, United States*

57   *University of Cincinnati, Cincinnati, OH, United States*

58   *University of Maryland, College Park, MD, United States*

59   *Syracuse University, Syracuse, NY, United States*

60   *Pontifícia Universidade Católica do Rio de Janeiro (PUC-Rio), Rio de Janeiro, Brazil, associated to [2]*

61   *Institute of Particle Physics, Central China Normal University, Wuhan, Hubei, China, associated to [3]*

62   *Departamento de Fisica , Universidad Nacional de Colombia, Bogota, Colombia, associated to [8]*

63   *Institut für Physik, Universität Rostock, Rostock, Germany, associated to [11]*

64   *National Research Centre Kurchatov Institute, Moscow, Russia, associated to [31]*

65   *Yandex School of Data Analysis, Moscow, Russia, associated to [31]*

66   *Instituto de Fisica Corpuscular (IFIC), Universitat de Valencia-CSIC, Valencia, Spain, associated to [36]*

67   *Van Swinderen Institute, University of Groningen, Groningen, The Netherlands, associated to [41]*

68   *Celal Bayar University, Manisa, Turkey, associated to [38]*

a   *Universidade Federal do Triângulo Mineiro (UFTM), Uberaba-MG, Brazil*

b   *P.N. Lebedev Physical Institute, Russian Academy of Science (LPI RAS), Moscow, Russia*

c   *Università di Bari, Bari, Italy*

d   *Università di Bologna, Bologna, Italy*

e   *Università di Cagliari, Cagliari, Italy*

f   *Università di Ferrara, Ferrara, Italy*

g   *Università di Firenze, Firenze, Italy*

h   *Università di Urbino, Urbino, Italy*

i   *Università di Modena e Reggio Emilia, Modena, Italy*

j   *Università di Genova, Genova, Italy*

[k] *Università di Milano Bicocca, Milano, Italy*

[l] *Università di Roma Tor Vergata, Roma, Italy*

[m] *Università di Roma La Sapienza, Roma, Italy*

[n] *Università della Basilicata, Potenza, Italy*

[o] *AGH - University of Science and Technology, Faculty of Computer Science, Electronics and Telecommunications, Kraków, Poland*

[p] *LIFAELS, La Salle, Universitat Ramon Llull, Barcelona, Spain*

[q] *Hanoi University of Science, Hanoi, Viet Nam*

[r] *Università di Padova, Padova, Italy*

[s] *Università di Pisa, Pisa, Italy*

[t] *Scuola Normale Superiore, Pisa, Italy*

[u] *Università degli Studi di Milano, Milano, Italy*

[v] *Politecnico di Milano, Milano, Italy*